35th Annual International Conference of the IEEE EMBS
Osaka, Japan, 3 - 7 July, 2013

Modeling intrinsic electrophysiology of AII amacrine cells: preliminary results

Nick Apollo[1,4], David B. Grayden[1,2,3,4], Anthony N. Burkitt[1,2,3,4], Hamish Meffin[1,2,4], Tatiana Kameneva[1,2,4,*]

***Abstract*— In patients who have lost their photoreceptors due to retinal degenerative diseases, it is possible to restore rudimentary vision by electrically stimulating surviving neurons. AII amacrine cells, which reside in the inner plexiform layer, split the signal from rod bipolar cells into ON and OFF cone pathways. As a result, it is of interest to develop a computational model to aid in the understanding of how these cells respond to the electrical stimulation delivered by a prosthetic implant. The aim of this work is to develop and constrain parameters in a single-compartment model of an AII amacrine cell using data from whole-cell patch clamp recordings. This model will be used to explore responses of AII amacrine cells to electrical stimulation. Single-compartment Hodgkin-Huxley-type neural models are simulated in the NEURON environment. Simulations showed successful reproduction of the potassium current-voltage relationship and some of the spiking properties observed in vitro.**

I. INTRODUCTION

Amacrine cells are the interneurons neurons located in the inner plexiform layer of the retina. Amacrine cells integrate, modulate and transmit visual information from the bipolar to ganglion cells. The AII amacrine cells are the main carriers of rod signals to the ganglion cells. An AII cell synapses with many rod bipolar cells, integrates their signals and then transmits this information to cone ON and OFF bipolar cells. The AII neurons connect onto the axon terminals of ON cone bipolar cells via electrical synapses (gap junctions) and form inhibitory chemical synapses onto OFF cone bipolar cells [8]. These cone bipolar cells synapse onto the ganglion cells, see Fig. 1, based on data from [8]. The AII neurons are the most numerous amacrine cells in the retina [10]. The density of AII amacrine cells is maximal in the parafovea region and then declines slowly with eccentricity. The density decreases from 5,736 cell bodies/mm^2 centrally to 820 cell bodies/mm^2 in peripheral retina.

In people who have lost their photoreceptors due to age-related macular degeneration or retinitis pigmentosa, a large number of neurons survive. By targeting surviving neurons with electrical stimulation, it is possible to restore functional vision to blind people [14]. Currently, epiretinal visual implants aim to be placed over the foveal region (a shallow depression in the center of the macula) to achieve higher visual acuity. The fovea is approximately 1.5 mm in diameter and the width of the parafoveal area is approximately 0.5 mm. Given the large size of a visual implant compared to the diameter of a fovea, an implant usually covers the parafovea region where the density of rods is maximum. For a successful visual prosthesis, it would be desirable to mimic the information processing of a healthy retina. In particular, it is important to stimulate the ON and OFF visual pathways independently. It is possible, that some AII cells will be stimulated directly with electrical stimulation. Given that AII amacrine cells split the signal from the rod bipolar cells into ON and OFF cone pathways (see Fig. 1), it would be desirable to understand how these cells respond to electrical stimulation.

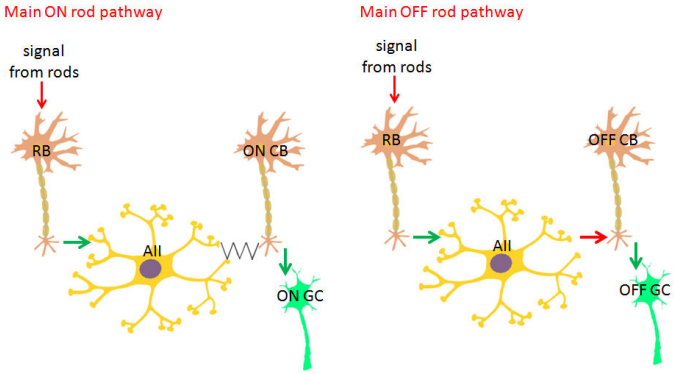

Fig. 1. Visual signal transmission in the mammalian retina. In figure: RB = rod bipolar cell, CB = cone bipolar cell (respectively ON or OFF), AII = AII amacrine cell, GC = ganglion cell (respectively ON or OFF), red arrows represent inhibitory synapses, green arrows represent excitatory synapses. Cartoons of neurons are taken from the open clipart library http://openclipart.org and do not represent the correct morphology of retinal neurons.

Voltage-gated currents in the AII amacrine cells have been studied in [1], [9], [7], [13]. The presence of potassium currents, I_{K} and $I_{\mathrm{K,A}}$, in the AII cells have been confirmed in [1], [9]. The sodium channel, I_{Na}, in AII cells was studied in [1], [9], [6], [7], [13]. The calcium channel, I_{Ca}, in these cells was characterized in [9]. Note that it is difficult to study ion currents in an isolated AII amacrine cell due to extensive gap junctions with ON bipolar cells and with other AII amacrine cells. To deal with the problem of the coupling between cells, the authors in [1] modulated the extent of coupling by dopamine and confirmed by staining that individual amacrine cells were isolated (refer to Fig. 2.b in [1]). We base our study of ion channels in AII

[1] NeuroEngineering Laboratory, Department of Electrical Electronic Engineering, The University of Melbourne. [2] NICTA Victoria Research Lab. [3] Bionics Institute, East Melbourne. [4] Centre for Neural Engineering, The University of Melbourne. *tkam@unimelb.edu.au

978-1-4577-0216-7/13/$26.00 ©2013 IEEE

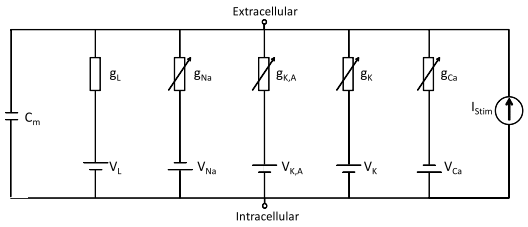

Fig. 2. Single-compartment model of AII amacrine cell: equivalent circuit model. For Kirchoffs current law summation of equivalent circuit, see (1).

amacrine based on experimental data obtained in [1]. The model has five voltage-gated currents that were characterized from earlier voltage-clamp data [2]. It includes a leakage current to match the input resistance of AII amacrine cells.

II. METHODS

A. Model description

To explore the role played by $I_{\rm K}$, $I_{\rm K,A}$, $I_{\rm Na}$, and $I_{\rm Ca}$ in the generation of AII amacrine cells' response, the dynamics of the ionic currents were described using Hodgkin-Huxley-type equations. Experimental data from [1] was used to constraint the model. The AII amacrine cells' ionic currents were summed using Kirchoff's law:

$$C_{\rm m}\frac{dV}{dt} = \bar{g}_{\rm L}(V-V_{\rm L})+\bar{g}_{\rm Na}m^3h(V-V_{\rm Na})+\bar{g}_{\rm Ca}c^3(V-V_{\rm Ca}) +(\bar{g}_{\rm K}n^4+\bar{g}_{\rm K,A}a^3h_{\rm A})(V-V_{\rm K})+I_{\rm stim}, \quad (1)$$

where V is the membrane potential, $C_{\rm m}$ is the specific capacitance of the membrane, $\bar{g}$ is the maximum conductance of an ionic current defined by the subscript, and $I_{\rm stim}$ is the intracellular stimulation current. The equivalent circuit model is given in Fig. 2. Delayed rectifier and A-type potassium currents had dynamics the same as in [2], unless overwise stated. Leak conductance was adjusted to reproduce experimentally observable input resistance in AII amacrine cells [11]. Sodium and calcium current dynamics were modified to replicate the lower level of activation of these currents in AII cells compared to retinal ganglion cells [1], [9]. The constrained sets of conductances of ionic currents were based on the intrinsic electrophysiology of AII cells. Morphological cell properties (soma diameter = 9 μm; soma length= 31.83 μm) and passive membrane parameters (C_m=1 μF/cm^2; $g_L = 2.44\times10^{-5}$ S/cm^2) were adapted from [1], [11]. Parameters for (1) that used in simulation were taken the same as in [2]. $\bar{g}_{\rm Na}$,$\bar{g}_{\rm K}$, $[10^{-15}, 10^{-2}]\bar{g}_{\rm K,A}$, and $\bar{g}_{\rm Ca}$ vary in the range $[10^{-15}, 10^{-2}]$.

Gating variables m, h, c, n, a of the voltage-gated ionic currents in (1) reflect the opening and closing of the ionic channels and satisfy the following: $\frac{dx}{dt} = -(\alpha_x+\beta_x)x+\alpha_x$, where x is the gating variable. The expressions for the gating variables are given in in Table 1. Note, in our simulations $A = 70$ mV in α_m for the sodium current and $B = 53$ mV in α_c for the calcium channel, while $A = 30$ mV and $B = 13$ mV in the original Fohlmeister and Miller study [2]. According to [1], the sodium channel activation range is shifted to a lower activation range in the amacrine cells compared to the ganglion cells. Activation range for sodium channels in AII amacrine cells is -55 to -60 mV, while in ganglion cells sodium currents first appear at -45 mV. Similarly, it was shown in [9] that the activation threshold of Ca^{2+} currents and their voltage of maximal activation are more negative than those reported for the majority of other high-voltage activated Ca^{2+} currents. Modification of the parameters A, B as above allowed us to shift the activation range of Na^{2+} and Ca^{+} currents by 30 mV.

Table 1. Rate constants for voltage-gated ion channels. V is measured in mV.

Na^+	$\alpha_m = \frac{-0.6(V+A)}{e^{-0.1(V+A)}-1}$	$\beta_m = 20e^{-(V+55)/18}$
	$\alpha_h = 0.4e^{-(V+50)/20}$	$\beta_h = \frac{6}{1+e^{-0.1(V+20)}}$
Ca^{2+}	$\alpha_c = \frac{-0.3(V+B)}{e^{-0.1(V+B)}-1}$	$\beta_c = 10e^{-(V+38)/18}$
K^+	$\alpha_n = \frac{-0.02(V+40)}{e^{-0.1(V+40)}-1}$	$\beta_n = 0.4e^{-(V+50)/80}$
K,A	$\alpha_a = \frac{-0.006(V+90)}{e^{-0.1(V+90)}-1}$	$\beta_a = 0.1e^{-(V+30)/10}$
	$\alpha_{h_{\rm A}} = 0.04e^{-(V+70)/20}$	$\beta_{h_{\rm A}} = \frac{0.6}{1+e^{-0.1(V+40)}}$

III. MODEL CONSTRAINTS

The following experimental data was used to constrain the model. First, to constrain the values of K^+ and K_A^+ conductances, the data presented in Figs. 9a, 9b in [1] was used, in particular, the response of the cells to the voltage-clamp steps of 60 ms duration. Simulated voltage dependence of the peak and sustained responses were compared to the experimental values. Voltage dependencies of the sustained response was measured 55 ms after depolarization. To account for the variability in ion conductances between individual cells *in vitro*, the constraints at each voltage step were taken as a range that included the experimental values, refer to Table 2. For these simulations Na^+ and Ca^{2+} conductances were set to zero to replicate Na^+ and Ca^{2+} channel blockage.

Second, to constrain the value of Ca^{2+} conductance, the data presented in Fig. 4c in [1] was used. In particular, the level of depolarization when the cell is injected with 25 pA current of 500 ms duration was used for the model constraining, refer to Table 2. For these simulations, potassium conductances were restricted to vary in the range that satisfied the experiment described above. Na^+ conductances was set to zero to replicate tetrodotoxin application.

Last, to constrain the value of Na^+ conductance, spiking properties observed *in vitro*, refer to Figs. 4b, 5b in [1], were used. For these simulations, K^+, K,A^+ and Ca^{2+} conductances were restricted to vary in the range that satisfied the experiments described above. For the list of model constraints, see Table 2.

The parameter space for $\bar{g}_{\rm Na}$, $\bar{g}_{\rm K}$, $\bar{g}_{\rm K,A}$, $\bar{g}_{\rm Ca}$ was searched using logarithmic steps (at each step the value was increased by a factor of 2) from $\bar{g}_T = 10^{-15}$ S/cm^2 to $\bar{g}_T = 0.1$ S/cm^2. A parameter search for the ionic conductances was performed in the NEURON environment [3]. Python and

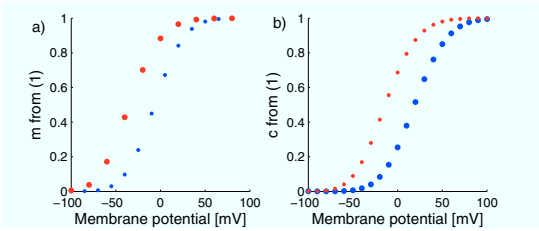

Fig. 3. Simulation results showing a shift in the sodium and potassium currents to the lower activation range in the amacrine cells compared to the ganglion cells. a) NA^+ channel inactivation. b) Ca^+ channel inactivation. Red: steady-state values with modified gating parameters; blue: original steady-state values, observed in ganglion cells in [2].

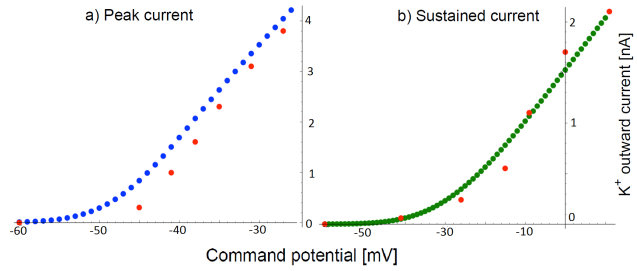

Fig. 4. Simulation of th peak (a) and sustained (b) potassium currents as a function of membrane voltage compared with experimental values [1]. Vertical axis is a total potassium currents and leak current, $I_{\mathrm{K}} + I_{\mathrm{K,A}} + I_{\mathrm{L}}$ [nA] and horizontal axis is the command potential (mV). Red dots: experimental values. Green dots: simulation results. Values used to plot peak current in this figure: $\bar{g}_{\mathrm{K}} = 2 \times 10^{-3}$ S/cm^2, $\bar{g}_{\mathrm{K,A}} = 0.21$ S/cm^2, $\bar{g}_{\mathrm{L}} = 2.44 \times 10^{-3}$ S/cm^2, $\bar{g}_{\mathrm{Na}} = \bar{g}_{\mathrm{Ca}} = 0$ S/cm^2. Values used to plot sustained current in this figure: $\bar{g}_{\mathrm{K}} = 4 \times 10^{-3}$ S/cm^2, $\bar{g}_{\mathrm{K,A}} = 0.01$ S/cm^2, $\bar{g}_{\mathrm{L}} = 2.44 \times 10^{-3}$ S/cm^2, $\bar{g}_{\mathrm{Na}} = \bar{g}_{\mathrm{Ca}} = 0$ S/cm^2.

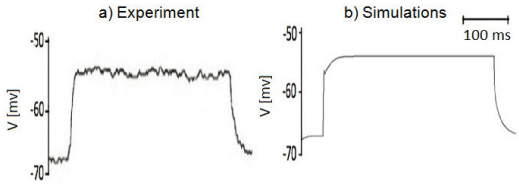

Fig. 5. Simulation of the current-clamp experiment from [1]. Membrane potential as a function of time in response to 30 pA current injection of 400 ms duration after 50 ms delay. During the experiment tetrodotoxin was administered (i.e., $\bar{g}_{\mathrm{Na}} = 0$). a) Experimental results. b) Simulations. Values used in simulations: $\bar{g}_{\mathrm{K}} = 10^{-5}$ S/cm^2, $\bar{g}_{\mathrm{K,A}} = 0.21$ S/cm^2, $\bar{g}_{\mathrm{L}} = 2.44 \times 10^{-3}$ S/cm^2, $\bar{g}_{\mathrm{Ca}} = 10^{-6}$ S/cm^2, $\bar{g}_{\mathrm{Na}} = 0$ S/cm^2.

Matlab codes were used to analyze and plot the results. All values were initialized at -65 mV value for the membrane potential, time step 0.025 ms was used in simulations.

To reproduce the current-voltage relations described in the first experiment above, a transmembrane current conversion was done. Currents in [1] are reported in absolute magnitudes (nA). However, current-clamp experiments in the NEURON environment assume current density (mA/cm^2). In order to convert the current values, the following adjustment was made: $I_{\mathrm{exp}} = I_{\mathrm{N}} A_{\mathrm{surf}}$, where I_{exp} is the value reported in [1], I_{N} is the current density value yielded by NEURON (mA/cm^2), A_{surf} is a surface area of an AII amacrine cell (900 micron squared).

IV. RESULTS

The inactivation dynamics for Na^+ and Ca^{2+} currents (variables m and c from (1), respectively) are given in Fig. 3. Note the shift to a more negative activation range when the gating parameters for these current are modified as described in Methods. Simulation led to successful reproduction of the potassium currents current-voltage relationship observed *in vitro* by [1]. Parameters that satisfied voltage-clamp experiments for the peak potassium current were in the following range: $\bar{g}_{\mathrm{K}} \in [2 \times 10^{-3}, 9 \times 10^{-3}]$ S/cm^2, $\bar{g}_{\mathrm{K,A}} = 0.21$ S/cm^2. Parameters that satisfied voltage-clamp experiments for the sustained potassium current were in the following range: $\bar{g}_{\mathrm{K}} \in [3 \times 10^{-3}, 4 \times 10^{-3}]$ S/cm^2, $\bar{g}_{\mathrm{K,A}} \in [0.11, 0.31]$ S/cm^2. A comparison of the experimental results and simulations is given in Fig. 4. Given the potassium conductances in the range that satisfied the experiment described above and zero Na^+ conductance (to replicate sodium channel blockage), we were able to reproduce the level of depolarization of AII amacrine cells observed *in vitro*. Parameters that satisfied the current-clamp experiment described in [1] were in the following range: $\bar{g}_{\mathrm{K}} \in [1 \times 10^{-9}, 0.2]$ S/cm^2, $\bar{g}_{\mathrm{K,A}} \in [0.1, 0.9]$ S/cm^2, $\bar{g}_{\mathrm{Ca}} \in [1 \times 10^{-6}, 1 \times 10^{-2}]$. A comparison of the experimental results and simulations is given in Fig. 5. Parameter search for Na^+ conductance did not lead to successful reproduction of graded potentials observed experimentally in [1]. We were able to reproduce spiking and oscillations in amacrine cells (data not shown due to space constraints), however the the frequency of spiking and subthreshold oscillation was much greater than the frequency of graded potential observed *in vitro*. We found that an increase in the Ca^{2+} conductance led to an increase in the amplitude of the spikes (data not shown due to space constraints).

By reducing the surface area of the cell by half, adjusting the kinetics of sodium and potassium currents (Na^+ inactivation $\alpha_h/3.5$, $\beta_h/3.5$; K^+ activation $\alpha_n/5$, $\beta_n/5$), leak reversal potential and conductance ($V_{\mathrm{L}} = -70$ mV, $\bar{g}_{\mathrm{L}} = 10^{-3}$ S/cm^2), we were able to reproduce spiking similar in amplitude and frequency to [1], see Fig. 6. This result requires further investigation.

V. DISCUSSION

We presented a model of AII amacrine cells that is able to capture some of the intrinsic electrophysiological behavior of these neurons as reported in [1]. Using systematic parameter search for the values of the ionic conductances, we were able to reproduce the voltage-current relationship for potassium currents and the level of depolarization under a current clamp. Our results on spiking properties of AII cells require further investigation.

Kinetics of sodium, calcium, delayed rectifier, and A-type potassium currents were based on experimental data from tiger salamander ganglion cells. As discussed above, kinetics of sodium and calcium channels have been shown to be different in AII amacrine cells compared to ganglion cells. In

Table 2. Model constraints.

Experiment	**Experim data**	**Constraints**
Voltage clamp	$I^{\text{exper}}_{\text{K+K,A,peak}} =$	$I_{\text{K+K,A,peak}} =$
Duration 60ms	3.8nA at -28mV	$I^{\text{exper}}_{\text{K+K,A,peak}}$
Peak current	3.1nA at -31mV	± 0.5mV
	2.4nA at -34mV	for all V
	1.7nA at -39mV	
	1nA at -42mV	
	0.3nA at -45mV	
	0nA at -60mV	
Voltage clamp	$I^{\text{exper}}_{\text{K+K,A,sus}} =$	$I_{\text{K+K,A,sus}} =$
Duration 60ms	2.1nA at 11mV	$I^{\text{exper}}_{\text{K+K,A,peak}}$
Sust current	1.7nA at 0mV	± 0.5mV
	1.1nA at -9mV	for all V
	0.7nA at -15mV	
	0.6nA at -26mV	
	0nA at -41mV	
Current clamp	No spiking	No spiking
$I_{\text{stim}} = 30$ pA	$V \in$	$V \in$
Duration 400ms	$[-56, -55]$mV	$[-58, -52]$mV
TTX application		
Current clamp	Number spikes	Number spikes
$I_{\text{stim}} = 25$ pA	$\in [10, 12]$	$\in [6, 20]$
Duration 400ms	Spike amp	Spike amp
	$\in [5, 10]$mV	$\in [5, 20]$mV

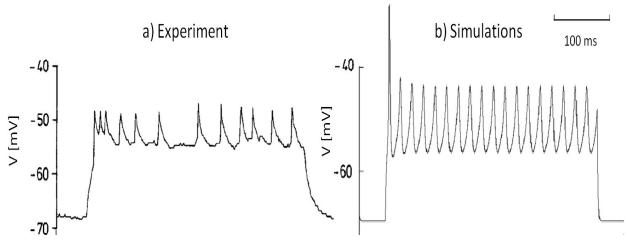

Fig. 6. Graded potential in AII amacrine cells. a) Experimental results. b) Simulations. Surface area of the cell, kinetics of sodium and potassium currents, leak reversal potential and conductance were modified as discussed in the text. Values used in simulations: $\bar{g}_{\text{K}} = 1 \times 10^{-5}$ S/cm^2, $\bar{g}_{\text{K,A}} = 2 \times 10^{-3}$ S/cm^2, $\bar{g}_{\text{L}} = 1 \times 10^{-6}$ S/cm^2, $\bar{g}_{\text{Na}} = 0.0059$ S/cm^2, $\bar{g}_{\text{Ca}} = 1 \times 10^{-6}$ S/cm^2.

order to reproduce amacrine cell spikelets observed *in vitro*, a modification of the channel kinetics from [2] is required. Due to the scarcity of the experimental data on the ion channel subtypes in AII amacrine cells, the model from [2] was used in this study.

Most neurons integrate dendritic synaptic input into a train of action potentials that originated at the axon initial segment. However, AII neurons do not fire action potentials; they have been shown to have intrinsic oscillations and generate graded potentials [7]. Amacrine cells do not have an axon, they both receive and transmit the signals via dendrites. Spike origin in these neurons remains unclear.

Sodium channels have been found in dendrites of AII amacrine cells [1], [7]. Some studies report that sodium channels reside in the compartments far enough electrotonically from the soma to provide an independent site for action potentials [1]. In this study, we have used a single-compartment Hodgkin-Huxley type neuron. While a single compartment model is sufficient for this study, extending the model to a more anatomically accurate, multiple compartment model is required to investigate this phenomenon.

To investigate responses of AII amacrine cells to various retinal prosthesis stimulation strategies, the model reported here needs to be improved and then validated on the data not used to constrain the parameters. For many visual implants, the aim is to achieve maximum resolution (high acuity). Given a large number of AII cells connect via gap junctions, a large area of the retina will be activated even if a small number of the amacrine cells is stimulated initially (current spread via electrical synapses). Simulation of an array of AII somas interconnected by gap junctions is reported in [6]. However, this study did not investigated the firing patterns and intrinsic electrophysiology of AII neurons (only sodium, potassium and leak current were used for modeling). A computational study on the role of gap junctions is reported in [5]. Consequences of the electrical coupling on the resolution of a visual implant is left for a future study. Note that althought in this study we do not investigate the effect of extracellular stimulation (which is used with visual implants), the model presented in this study is the first step towards this aim.

VI. Acknowledgments

This research was supported by the Australian Research Council through its Special Research Initiative in Bionic Vision Science and Technology grant to Bionic Vision Australia. The Bionic Ear Institute acknowledges the support it receives from the Victorian Government through its Operational Infrastructure Support Program. Nick Apollo was funded by the Fullbright and Whitaker Fellowships.

References

[1] Boos R., Schneider H., Wassle H. Voltage- and transmitter-gated currents of AII-Amacrine cells in a slice preparation of the rat retina. *J. Neurosci.,* 13(7): 28742888, 1993.

[2] Fohlmeister J. F. and Miller R. F. Impulse encoding menchanisms of ganglion cells in the tiger salamander retina. *J. Neurophysiol.,* 78: 1935-1947, 1997.

[3] Hines M. NEURON a program for simulation of nerve equations. *In: Neural Systems: Analysis and Modeling, edited by F. Eckman. Norwell, MA: Kluwer Academic Publishers*, 1993.

[4] Osterberg G. Topography of the layer of rods and cones in the human retina. *Acta. Ophthal. Suppl.*, 6: 1103, 1935.

[5] Publio R., Oliveira R.F., Roque A.C. A computational study on the role of gap junctions and rod Ih conductance in the enhancement of the dynamic range of the retina. *PLoS ONE,* 4(9), e6970, 2009.

[6] Smith R.G., Vardi N. Simulation of the AII amacrine cell of mammalian retina:Functional consequences of electrical coupling and regenerative membrane properties. *Vis. Neurosci.,* 12: 851-860, 1995.

[7] Tian M., Jarsky T.,Murphy G.J., Rieke F., Singer J.H. Voltage-gated Na channels in AII amacrine cells accelerate scotopic light responses mediated by the rod bipolar cell pathway. *J. Neurosci.,* 30(11): 4650-4669, 2010.

[8] Wassle H. Parallel processing in mammalian retina. *Nature Reviews Neurosci.,* 5: 1-11, 2004.

[9] Habermann C.J., O'Brien B.J., Wassle H., Protti D.A. AII amacrine cells express L-type calcium channels at their output synapses. *J. Neurosci,* 23(17): 6904 - 6913, 2003.

[10] Vaney D.I., The mosaic of amacrine cells in the mammalian retina. *Prog. Retinal Res.,* 9: 49-100, 1990.

[11] Veruki M.L., Oltedal L., Harveit E. Electrical coupling and passive membrane properties of AII amacrine cells. *J. Neurophysiol.*, 103: 1456-1466, 2010.

[12] Wassle H., Grunert I., Chun M-H, Boycott B.B. The Rod Pathway of the Macaque Monkey Retina: Identification of AII-Amacrine Cells With Antibodies Against Calretinin. *J. Comp. Biol.,* 361: 537 - 551, 1995.

[13] Wu C., Ivanova E., Cui J., Lu Q., Pan Z.-H. Action potential generation at an axon initial segment-like process in the axonless retinal AII amacrine cell. *J. Neurosci.,* 31(41): 14654-14659, 2011.

[14] E. Zrenner. Will retinal implants restore vision? *Science,* 295: 1022-1025, 2002.